# A Study of Unbalanced Magnetic Pull in Brushless Doubly Fed Machines

**Abdi Jalebi, S., Abdi, E. & McMahon, R.**



**Original citation & hyperlink:**
Abdi Jalebi, S, Abdi, E & McMahon, R 2015, 'A Study of Unbalanced Magnetic Pull in Brushless Doubly Fed Machines' IEEE Transactions on Energy Conversion, vol. 30, no. 3, pp. 1218-1227.
https://dx.doi.org/10.1109/TEC.2015.2394912

DOI 10.1109/TEC.2015.2394912
ISSN 0885-8969

Publisher: Institute of Electrical and Electronics Engineers (IEEE)

# A Study of Unbalanced Magnetic Pull in Brushless Doubly Fed Machines

Salman Abdi, Ehsan Abdi, *Senior Member, IEEE,* and Richard McMahon

***Abstract*— This paper studies the unbalanced magnetic pull (UMP) in the Brushless Doubly-Fed Machine (BDFM), caused by both static and dynamic rotor eccentricities. Several parallel winding designs for the two stator windings are proposed and the practicality of such designs is discussed with respect to direct coupling between the stator windings and with rotor undesirable harmonic fields. Once practical parallel winding designs are established, their effects on reducing deflection as a result of static and dynamic eccentricities are shown and compared with series wound stator. The study has been carried out on a prototype D400 250 kW BDFM.**

***Index Terms*— Brushless doubly fed machine (BDFM), finite element (FE) analysis, unbalanced magnetic pull (UMP), rotor eccentricity, parallel winding**

## I. Introduction

The BDFM is an alternative to the well-established Doubly-Fed Induction Generator (DFIG) for use in wind turbines as it retains the benefit of utilizing a fractional-size converter, but it also offers higher reliability and lower maintenance costs than the DFIG due to absence of brush gear and slip-rings [1]. In addition, the BDFM is intrinsically a medium-speed machine, enabling the use of a simplified one or two-stage gearbox, hence reducing the cost of the overall drivetrain and giving further reliability improvement.

The modern BDFM as a variable speed drive or generator comprises two electrically separate stator windings, one connected directly to the grid, called the power winding (PW), and the other supplied from a variable voltage and frequency converter, called the control winding (CW). The pole numbers are selected in a way to avoid direct transformer coupling between the stator windings. The coupling between the windings is therefore through the rotor [2]. The rotor is specially designed to couple to the two air-gap fields associated with the two stator windings, the nested-loop design being commonly used [3]. The normal mode of BDFM operation is as a synchronous machine with the rotor rotating at a speed determined by the winding pole numbers and the mains and converter frequencies [2].

As with all induction type machines, characterized by relatively small air gaps, the strong magnetic fields across the air gap exert considerable forces on the iron parts of the machine. These cause time-varying deflections on the machine surface which lead to vibration and acoustic noise. One source of producing deflection is unbalanced magnetic pull (UMP), which can be mathematically shown as the interaction between two air gap flux waves with pole-pair numbers differing by one [4].

Unlike the induction motor, which has a magnetic field dominated by a single pole number component, the BDFM has principle field components at two different pole numbers and the interaction of these two components leads to more complex deflection patterns than those occur in the induction machine [5].

The presence of rotor eccentricity in practical machines further modulates the field patterns, exacerbating the resulting vibration. An eccentric rotor motion occurs when the rotor axis is not aligned with the axis of the stator bore. Due to manufacturing tolerances, wear of bearings, and other reasons, some degree of rotor eccentricity is always present. Rotor whirling generates an electromagnetic force also known as UMP that acts between the rotor and stator. This force can be resolved into two components: the radial force, acting in the direction of the shortest air gap; and the tangential force, which is perpendicular to the radial force. The amplitude and direction of the latter force depend on the operating condition of the machine, whirling frequency and rotor radius. Acting roughly in the direction of the shortest air gap, UMP tends to further increase the eccentricity magnitude and may cause serious damage to the machine or even the whole drive. In addition, UMP acts as a major source of vibration and acoustic noise.

Parallel connection of stator coils is widely used to reduce UMP in electrical machines with nonuniform air gaps and its effects have been discussed in the literature, for example in [6]. Effectively, the variation of reluctance due to uneven air gap length causes circulating currents in the parallel paths, which improve the air gap flux distribution, hence reducing the deflection and UMP.

The effects of rotor eccentricity on machine performance and the use of parallel windings, as a way to suppress its effects, have been studied for induction machines [7]–[9], synchronous machines [10], switched reluctance machines [11] and permanent magnet machines [12]. But little work has been done on UMP and vibration analysis for the BDFM [5], [13]. Connecting the stator coils in parallel in a BDFM is not as straightforward as in other electrical machines. The main reason is that parallel connection of stator coils may lead direct coupling of stator windings if not considered carefully. The large circulating currents produced by direct coupling will cause significant losses and degrade machine performance.

A detailed study of UMP and its resultant displacement in stator back iron for the BDFM is presented in this paper taking the effects of rotor eccentricity into account. The key

S. Abdi and R. McMahon are with the Electrical Engineering Division, Cambridge University, Cambridge, CB3 0FA, UK (e-mail: s.abdi.jalebi@gmail.com; ram1@eng.cam.ac.uk)

E. Abdi is with Wind Technologies Limited, St Johns Innovation Park, Cambridge CB4 0WS, UK. (e-mail: ehsan.abdi@windtechnologies.com)

contribution of this paper is the assessment of the parallel connection of stator coils in the BDFM such that direct coupling is eliminated. This is particularly challenging when short pitched windings are used.

Analytical methods are commonly used to study the electromagnetic forces due to rotor eccentricity, for example in [8], [14], [15], however such methods are not sufficient when accurate assessment of rotor eccentricity, iron saturation effects, and stator and rotor slotting is required. In addition, the complex magnetic field pattern in the BDFM air gap resulting from the two stator fields with different pole numbers and frequencies makes an analytical study difficult. Time-stepping Finite Element (FE) modelling which has been verified experimentally for a D400 250 kW prototype BDFM is therefore utilized. FE analysis has been widely used, for example in [7], [9], [10], [12], [16], to study UMP and its resulting vibration in electrical machines. The drawback of FE modelling is that in the presence of eccentricity, there is no geometric symmetry, so the whole cross section of the machine must be modelled. This results in an FE mesh with a large number of elements as reported by others such as [17], [18] making the analysis time consuming.

## II. Prototype Machine Considered in This Study

The specifications of the 250 kW BDFM are shown in Table I. The D400 BDFM was constructed as a frame size 400 machine with the stack length of 820 mm. The stator windings were form wound from copper strips. The power winding was rated at 690 V, 178 A, at 50 Hz and the control winding was designed for 620 V at 18 Hz and rated at 73 A. Both stator windings were connected in delta. The rotor comprises six sets of nests each consisting of a number of concentric loops [19], the conductors being solid bars with one common end ring [20]. The magnetic properties for the iron were provided by the machine manufacturer. The D400 BDFM on test bed is shown in Fig. 1.

TABLE I: Specifications of the 250 kW D400 BDFM

| | |
|---|---|
| Frame size | 400 |
| PW pole number | 4 |
| PW rated voltage | 690V at 50 Hz (delta) |
| PW rated current | 178 A (line) |
| CW pole number | 8 |
| CW rated voltage | 620 V at 18 Hz (delta) |
| CW rated current | 73 A (line) |
| Speed range | 500 rpm ±36% |
| Rated torque | 3670 Nm |
| Rated power | 250 kW at 680 rpm |
| Efficiency (at full load) | > 95% |
| Stack length | 0.82 m |

## III. Magnetic Forces and Resulting Deflections

The radial forces exerted by the air gap magnetic field on the stator tooth tops are calculated. The effect of tangential forces

Fig. 1: 250 kW D400 BDFM (right front) on test bed

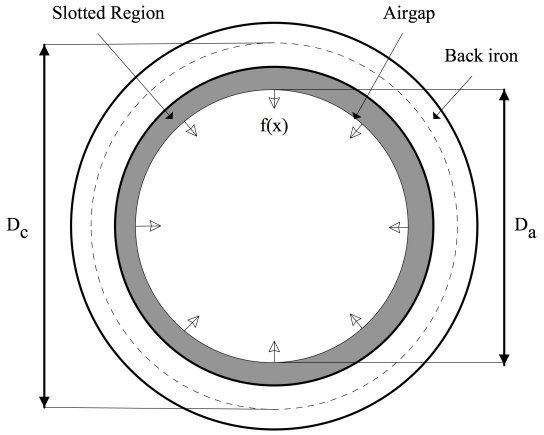


Fig. 2: BDFM Stator subjected to magnetic pull

on the teeth which ultimately exert torque to the machine's shaft are not considered in this analysis [5]. Fig. 2 shows the schematic of the BDFM stator. The air gap magnetic field is essentially the superposition of two field components, one with $2p_1$ poles, the mean absolute flux density of $\bar{B}_1$ rotating at $\omega_1$ $rad/s$ and another with $2p_2$ poles, $\bar{B}_2$ flux density rotating at $\omega_2$. The total flux density as a function of space angle and time is therefore:

$$B(\theta,t) = \frac{\pi}{2}[\bar{B}_1 \cos(p_1\theta+\omega_1 t+\phi_1)+\bar{B}_2 \cos(p_2\theta+\omega_2 t+\phi_2)] \quad (1)$$

where $\omega_1$ and $\omega_2$ are the frequencies of the two stator supplies, and $\phi_1$ and $\phi_2$ are phase offsets. Any harmonic field components created by the rotor structure, slotting, saturation and rotor eccentricity are ignored in (1). In Fig. 3, a typical air gap field for a 4/8 pole BDFM at the point where $t$ and $\phi$ terms are zero is shown in black, i.e. the smooth line. The field represents magnetic loading of 0.48 $T$ which is the design value for the 250 kW BDFM. The air gap flux density obtained from 2-D linear FE modelling which takes into account all the harmonic components mentioned above is also shown in Fig. 3 for a centric rotor. The magnetic field in the air gap exerts an

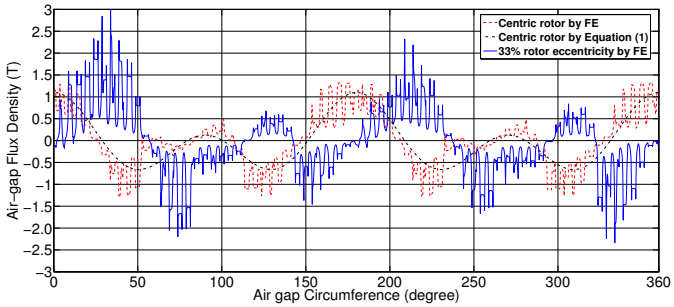


Fig. 3: Air gap flux density obtained from (1) and FE modelling when the rotor is centric and eccentric. Results are obtained from frozen fields at different times, so the relative phase shift is arbitrary.

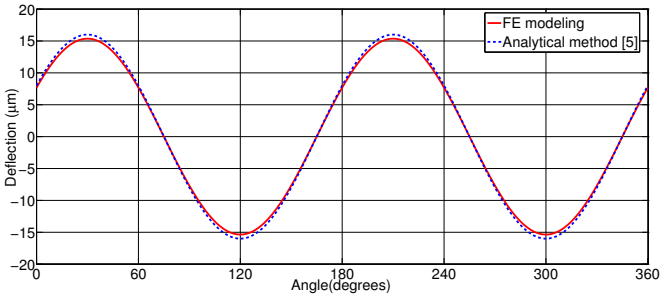


Fig. 4: Comparison of displacements in the stator back iron when the rotor is centric obtained from FE modelling and analytical method

inward force on the stator tooth top and an equal and opposite outwards force on the rotor tooth tops. At any point the force is related to the magnetic field strength by [21]

$$f = \frac{B^2(\theta,t)}{2\mu_0} \tag{2}$$

This force will cause the stator back iron to deflect which is estimated using 1-dimensional beam theory as proposed by Alger [22]. The force must be balanced by elastic deformation of the back iron and the frame. The force in the air gap may be replaced by an equivalent force at the central axis of the back iron (the dashed line in Fig. 2) given as a function of the mechanical angle by

$$f_b(\theta,t) = \frac{D_a}{D_c}\frac{B^2(\theta,t)}{2\mu_0} \tag{3}$$

where $D_a$ is the air gap diameter and $D_c$ is the diameter at the centre of the back iron. The force can be considered as the superposition of two components, the average force which causes a small deflection constant in $\theta$ and can be neglected [5], and the space varying component given by

$$f_b'(\theta,t) = f_b(\theta,t) - \frac{1}{2\pi}\int_0^{2\pi} f_b(\theta,t).d\theta \tag{4}$$

Next, the deflection resulted from this applied force can be calculated. The force is resisted mainly by the stator back iron, as the machine's frame makes negligible contribution to resisting the magnetic forces due to its much lower bending stiffness [5]. The shear stress $S$ in the beam is related to the force by

$$S(\theta,t) = \frac{D_c l}{2}\int f_b'(\theta,t).d\theta \tag{5}$$

The shear stress is the differential of the bending moment $M$ and therefore

$$M(\theta,t) = \frac{D_c}{2}\int S(\theta,t).d\theta \tag{6}$$

Finally the deflection, $v(\theta,t)$ due to the loading is given by the double integral of the bending moment

$$v(\theta,t) = -\frac{D_c^2}{4}\frac{12}{E_{ym} l y_c^3}\int\int M(\theta,t).d\theta \tag{7}$$

where $E_{ym}$ is the Young's Modulus of the material, $y_c$ is the core back depth and $l$ is the stator stack length. In the present study, the air gap flux density, $B(\theta,t)$, is obtained from FE modelling. Then from (2) to (7), the stator back iron displacement is obtained. Fig. 4 shows the deflection obtained from the method described above and from the experimentally verified analytical method given in [5]. As can be seen, there is close agreement between the two results, validating the approach used in this paper to calculate deflection.

## IV. Effects of Rotor Eccentricities

The radial forces acting on the surface of the rotor are very large but cancel each other when the rotor axis is aligned with the stator axis. Similarly, tangential forces are balanced such that only an axially rotating moment is produced. If the rotor is eccentric, then UMP occurs. The phenomenon can be described as an imbalance of the radial and tangential forces acting on the rotor (or stator) surface such that a net radial force is developed. This can result in vibration and noise, and increase the possibility of the stator and rotor contact.

The UMP due to eccentricity takes two forms: static and dynamic. Static UMP is caused by the rotor axis being positioned parallel to, rather than being on, the stator axis as a result of manufacturing tolerances. In this case, the rotor is rotating around its own axis, see Fig. 5. Dynamic UMP occurs when the rotor is precessing about the stator bore centre but not its own centre, see Fig. 6. This could be produced by manufacturing tolerances or rotor whirl near a critical speed. Different levels of static and dynamic eccentricities when the rotor is off-centre by 33%, 21%, and 7% of the nominal air gap length are considered in this study. The level of eccentricity referred to in the following text is always expressed as percentage of the nominal air gap length.

The air-gap magnetic flux density distribution frozen in time for a perfectly constructed BDFM with uniform air gap and specifications given in Table I, and the case when the rotor is statically eccentric by 33%, are shown in Fig. 3. It is obvious from the figure that some regions of the non-uniform air gap experience high level of flux density, up to 3 T. As shown in Fig. 7, this high flux density level results in a deflection which is significantly i.e. 18 times larger than the case of an ideally constructed machine. Therefore, the mitigation of UMP

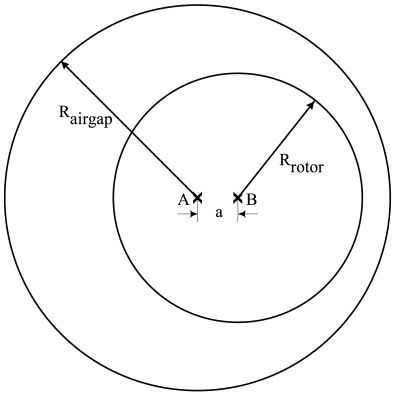


Fig. 5: Static eccentricity when the rotor centre (B) is not aligned with the stator centre (A). The position of B is constant with time and the level of eccentricity is 'a'.

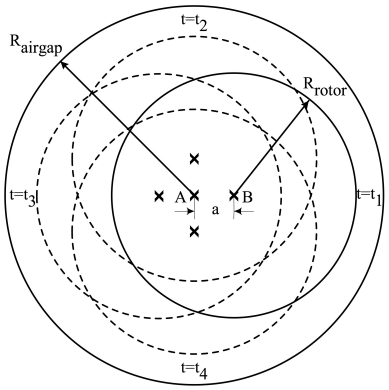


Fig. 6: Dynamic eccentricity when the rotor centre (B) is not aligned with the stator centre (A) . The position of B varies with time, but the level of eccentricity 'a' remains constant.

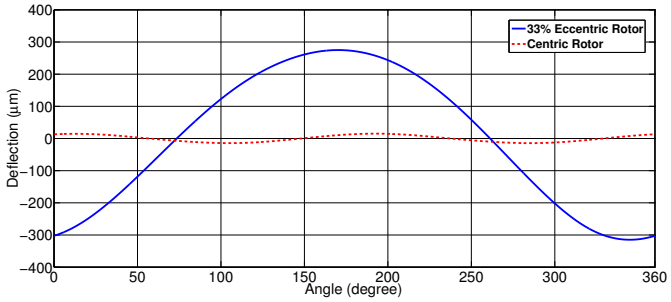


Fig. 7: Displacement in the stator back iron when the rotor is centric and when the rotor is 33% eccentric

is important in the BDFM if standard manufacturing tolerances are allowed; parallel connection of stator coils will be shown to be an effective way to reduce deflection.

## V. Stator Parallel Windings in Brushless Doubly Fed Machines

Paralleling the stator coils is a well-known practice to mitigate UMP in electrical machines caused by a non-uniform air gap. In the BDFM, the pole pair numbers for the PW and CW are typically chosen in a way that when their coils are connected in series, the net voltage in each phase of the PW and CW induced by direct coupling with the other winding's field is zero. Parallel connection of stator coils specially when short pitched windings are used can potentially lead to direct coupling between the two stator windings and hence, special care must be taken into account in the winding design. The induced voltage due to direct coupling of stator windings is calculated in the following section to assess various parallel winding designs.

### A. Induced voltage due to direct coupling

Two principle fields are generated in the BDFM air gap when the PW and CW are supplied with three-phase balanced voltages. They are given, when the rotor is stationary, by

$$B_{PW}(\theta,t) = \bar{B}_{PW}\cos(\omega_{s1}t - p_1\theta) \tag{8}$$

$$B_{CW}(\theta,t) = \bar{B}_{CW}\cos(\omega_{s2}t - p_2\theta) \tag{9}$$

where $\omega_{s1}$ and $\omega_{s2}$ are the PW and CW angular frequencies respectively, $\theta$ is the angle expressed in a coordinate reference frame fixed to the rotor, and $p_1$ and $p_2$ are the PW and CW pole pair numbers respectively. The magnetic flux linked by a single stator coil is obtained by

$$\phi = l\frac{d}{2}\int_{\alpha 1}^{\alpha 2} B(\theta,t).d\theta \tag{10}$$

where $l$ and $d$ are the lamination stack length and mean air gap diameter respectively. $\alpha_1$ and $\alpha_2$ are the angles representing the coil locations. From Faraday's law, the voltage induced in a single CW coil due to the $p_1$-pole air gap field is:

$$v_{coil}^{CW} = -N_{CW}\frac{d\phi_{PW}}{dt} = \frac{ld\bar{B}_{PW}\omega_{s1}}{2p_1}N_{CW}[ cos(\omega_{s1}t - p_1\alpha_2) - cos(\omega_{s1}t - p_1\alpha_1)] \tag{11}$$

Simillarly, the induced voltage in a single PW coil due to the $p_2$-pole air gap field is

$$v_{coil}^{PW} = \frac{ld\bar{B}_{CW}\omega_{s2}}{2p_2}N_{PW}[ cos(\omega_{s2}t - p_2\alpha_2) - cos(\omega_{s2}t - p_2\alpha_1)] \tag{12}$$

$N_{PW}$ and $N_{CW}$ are the number of PW and CW coil turns. The winding diagrams for the PW and CW in the 250 kW BDFM are shown in Figs. 8 and 9. Each coloured area comprises a number of slots containing coils of a single phase. The coils of each phase located in adjacent slots of a single winding layer are connected in series, creating a coil group. This is normal practice in the majority of winding configurations. Each coloured area i.e. $X_i$ and $\bar{X}_i$ in Figs. 8 and 9 therefore represents a coil group. The PW has four coil groups per phase, each with six series-connected coils and the stator CW has eight coil groups per phase, each with three series-connected coils. Therefore, the induced voltages across the m*th* PW coil group, $v_{U_m}^{PW}$ and n*th* CW coil group, $v_{A_n}^{CW}$ are:

$$v_{Um}^{PW} = \sum_{i=1}^{6} v_{U_m - i^{th}coil}^{PW} \tag{13}$$

$$v_{An}^{CW} = \sum_{i=1}^{3} v_{A_n - i^{th} coil}^{CW} \tag{14}$$

If the net induced voltage in a coil group from direct coupling with the other stator field, i.e. $v_{U_m}^{PW}$ or $v_{A_n}^{CW}$ is not zero, then sufficient number of coil groups must be connected in series to make the net sum to zero, hence eliminating the effect of direct coupling.

### *B. Parallel connection of coil groups when both PW and CW are short pitched*

Stator winding short pitching is widely used in electrical machines with double-layer winding construction. Short pitching reduces the harmonic content of the flux density in the air gap and consequently produces a more sinusoidal current linkage distribution than a full-pitch winding [23]. Most of the BDFMs built by the authors and others including the 250 kW BDFM have employed short-pitch windings, as shown in Figs 8 and 9.

However, the short pitch configuration causes each coil group to couple to the other stator field. But, series connection of all coil groups within a phase leads to a zero net induced voltage. With careful consideration, only the minimum number of coil groups can be connected in series to produce a net zero induced voltage from the other stator field. Then, these series connected coil groups can be connected in parallel without causing any direct coupling. Equations (13) and (14) are used to calculate the induced voltage in PW and CW coil groups and following results are obtained:

$$v_{U1}^{PW} = v_{U3}^{PW} = -v_{U2}^{PW} = -v_{U4}^{PW} \tag{15}$$

$$v_{A1}^{CW} = v_{A5}^{CW} = -v_{A3}^{CW} = -v_{A7}^{CW} \tag{16}$$

$$v_{A2}^{CW} = v_{A6}^{CW} = -v_{A4}^{CW} = -v_{A8}^{CW} \tag{17}$$

Figs. 10 and 11 show the position of the CW and PW coil groups related to the air gap field produced by the other stator winding, respectively. They show how the voltage in each of the coil groups is induced by the other stator field. From (15), (16) and (17), the PW coils can only be connected in parallel as shown in Fig. 12, but CW coils can have either of the arrangements shown in Fig. 13. The winding design shown in Fig. 13(a) for the CW is expected to be more effective in reducing deflection since it contains more parallel paths.

Though the winding connections proposed in Figs. 12 and 13 for the PW and CW will eliminate direct coupling between the stator windings, they may still have a strong net coupling with the undesirable harmonics of the rotor field, making them impractical. It will be shown in the following section that the CW connection proposed in Fig. 13(a) will suffer from this issue.

### *C. Undesirable time harmonics in stator windings due to rotor harmonics*

The 250 kW BDFM is modelled in FE in the synchronous mode of operation where its PW and CW are wound according to Figs. 12 and 13(a) respectively. The rotor is perfectly

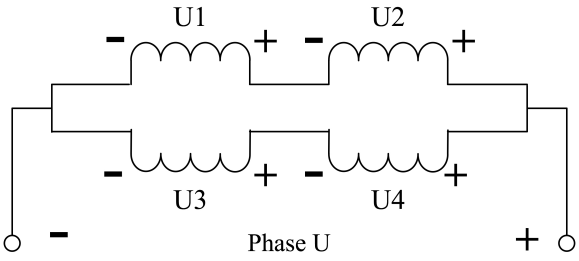


Fig. 12: Proposed connection of PW coil groups shown in Fig. 8 which eliminates the effect of direct coupling

constructed and the PW and CW are supplied at their rated voltages and frequencies, shown in Table I. Significant quantities of time harmonics is found in the CW currents when the machine reaches the steady state condition, as shown in Fig. 14. The largest harmonic is at 115 Hz with an amplitude of 48% of the main harmonic i.e. 15 Hz. This is caused by the coupling between undesirable rotor field harmonics and the CW coil groups, producing induced voltages that are not summed to zero through the proposed winding connection in Fig. 13(a). The extent of stator current harmonic content can be found by evaluating the winding factor ($K_w$). $K_w$ is affected by the winding configuration, and whether it is fully pitched or short pitched. In general, short pitched winding structures lead to more sinusoidal stator currents [23]. FE analysis reveals that rotor time harmonics are present and Fig. 15 shows the Fast Fourier Transform (FFT) of current harmonics in rotor loops. Suppose the rotor current harmonic with the frequency of $f_r^i$ can produce a rotor magnetic field with $p_r^j$ pole pair number, then the speed of this field with respect to the rotor frame is

$$n_{B_r}^{rot(i,j)} = \frac{f_r^i \times 60}{p_r^j} \tag{18}$$

in $rpm$. The stator however sees this field with the speed of

$$n_{B_r}^{st(i,j)} = n_{B_r}^{rot(i,j)} \pm n_r \tag{19}$$

where $n_r$ is the rotor shaft speed. If a stator coil couples with this field, the frequency of the induced current will be

$$f_{st}^{(f_r^i, p_r^j)} = n_{B_r}^{st(i,j)} \frac{p_r}{60} = f_r^i \pm p_r^j \frac{n_r}{60} \tag{20}$$

Using (20) and from the frequency of the current harmonics in a stator coil, the possible combinations of $f_r^i$ and $p_r^j$ can be obtained.

As shown in Fig. 14, the CW currents have a strong 115 Hz harmonic component. Using (20), the possible combinations of $f_r^i$ and $p_r^j$ are shown in Table II. It should be noted that not all of these combinations are realistic.

The nested-loop rotor produces various space harmonics, including $P_1$, $P_2$, $p_1 + nN_r$ and $p_2 + nN_r$, where $N_r$ is the number of rotor nests and is an integer [24]. Therefore, among the possible combinations given in Table II, only 4, 8, 16, 20, 32 and 56 pole-pairs exist.


Fig. 8: Stator PW Short pitched by three slots

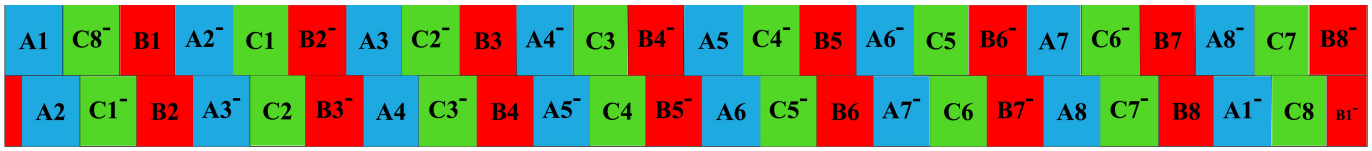


Fig. 9: Stator CW short pitched by one slot

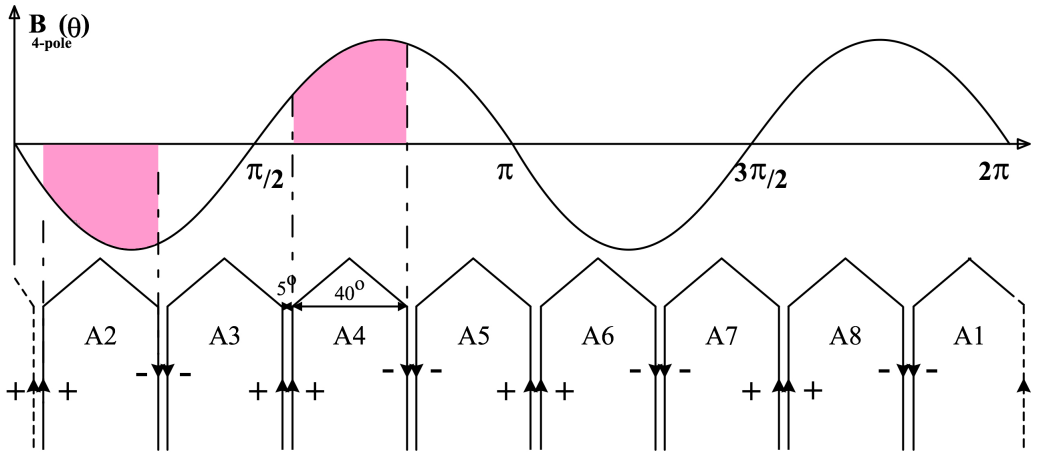


Fig. 10: 4-pole air gap field produced by the PW in the air gap, and the positions of CW coil groups. Series connection of coils A2 and A4 leads to zero net direct coupling

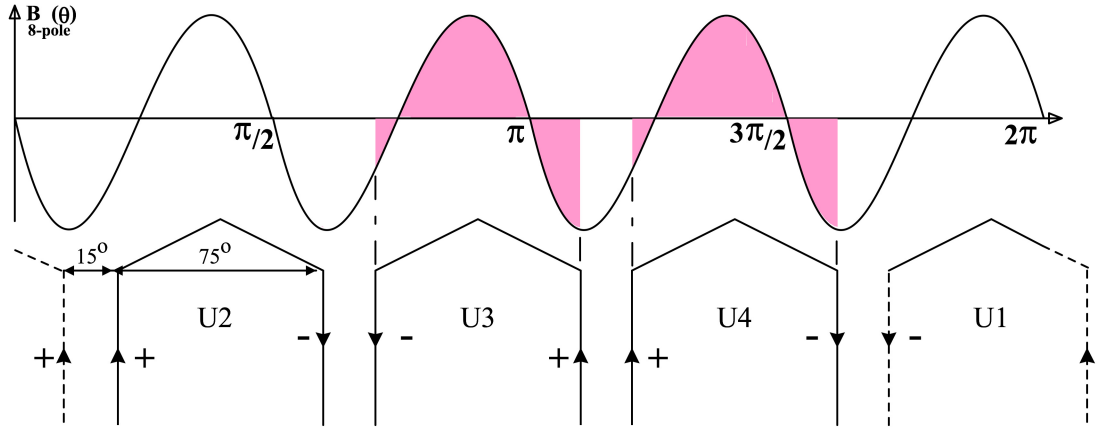


Fig. 11: 8-pole air gap field produced by the CW in the air gap, and the positions of PW coil groups. Series connection of coils U3 and U4 leads to zero net direct coupling

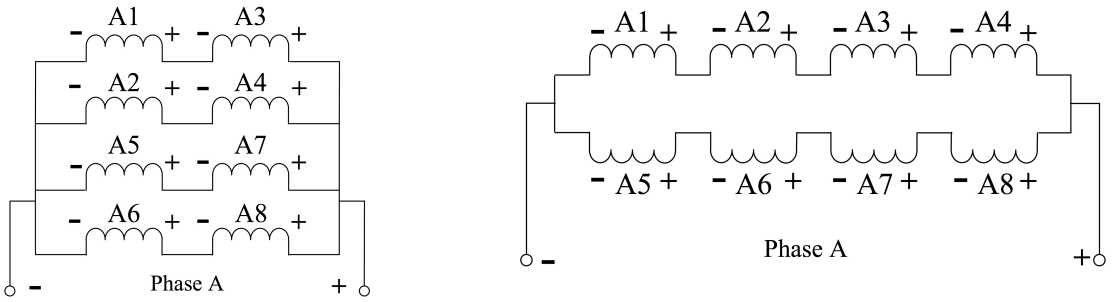


(a) (b)

Fig. 13: Two proposed connections of CW coil groups shown in Fig. 9 which eliminate the effects of direct coupling (a) with four parallel paths. (b) with two parallel paths.

TABLE II: Possible combinations of rotor current harmonics and the resulting field pole pair numbers producing a 115 Hz current harmonic in the CW.

| Case | 1 | 2 | 3 | 4 | 5 | 6 | 7 | 8 |
|---|---|---|---|---|---|---|---|---|
| $f_r^i(Hz)$ | 28.3 | 101.6 | 158.2 | 190.8 | 231.7 | 288.3 | 450.8 | 491.7 |
| $p_r^j$ | 8 | 20 | 4 | 7 | 32 | 16 | 31 | 56 |

Equations (11) to (14) can also be used to calculate the induced voltages in the CW coils when they are exposed to rotor magnetic field with pole numbers and frequencies given in Table II. The following results are obtained for Cases 1 and 2:

$$v_{A1}^{CW} = v_{A2}^{CW} = ... = v_{A8}^{CW} \tag{21}$$

and for Cases 4,5,6 and 8:

$$v_{A1}^{CW} = v_{A3}^{CW} = -v_{A2}^{CW} = -v_{A4}^{CW} \tag{22}$$

$$v_{A5}^{CW} = v_{A7}^{CW} = -v_{A6}^{CW} = -v_{A8}^{CW} \tag{23}$$

From (21) to (23) it can be shown that the CW design shown in Fig. 13(a) shows a net coupling to the rotor field harmonics and hence is not a practical design. However, the PW and CW winding designs shown in Figs. 12 and 13(b) do not couple to each other directly and to the rotor undesirable harmonic fields. The CW current for the winding design of Fig. 13(b) is shown in Fig. 14 and as can be seen, does not contain significant harmonics.

### *D. Parallel connection of coil groups when PW is fully pitched*

It is shown in [5] that the stator winding with lower pole number (PW in the case of the 250 kW BDFM) has a more significant contribution to the deflection and hence increasing the number of parallel paths in the lower pole number winding can result in reduction of stator back iron displacement and its consequent vibration effects.

If the PW coils are fully pitched, there will not be any direct coupling with the CW field and hence all coil groups can be connected in parallel, as shown in Fig. 16. The effect of higher number of parallel paths in the PW design on reducing deflection will be shown in section VII. It should be noted that harmonic content of the PW current is increased when a fully pitched structure is utilized.

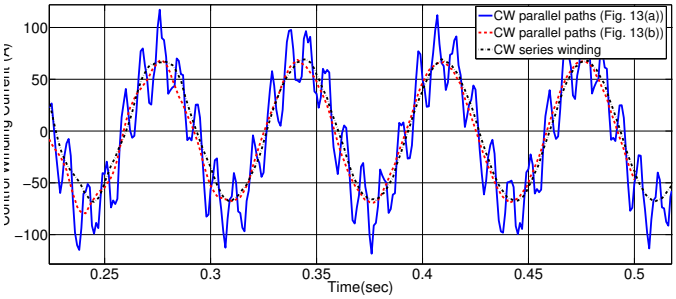


Fig. 14: Comparison of CW currents when its coils are connected in series, according to Figs. 13(a) and 13(b)

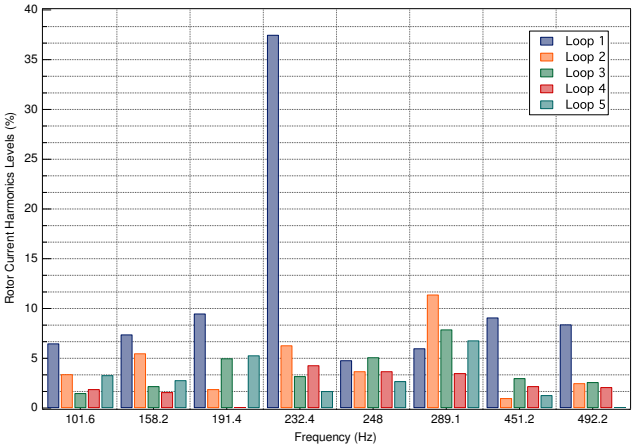


Fig. 15: FFT analysis of current harmonics in rotor loops. The amplitudes are expressed as percentage of the principle harmonic, i.e. 28.3 Hz in each loop.

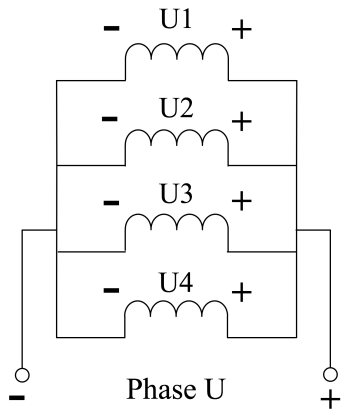


Fig. 16: Proposed connection of PW coil groups for a fully pitched winding.

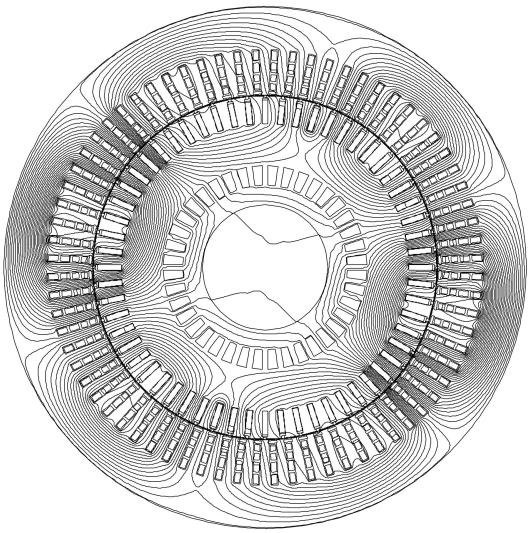

Fig. 17: Magnetic flux in the BDFM in synchronous mode of operation

## VI. Designs Considered in This Study

The 250 kW BDFM when operating in the synchronous mode is modelled in FE using a time stepping method. The FE models are verified by experimental results reported in [25]. The PW and CW are supplied at 50 Hz and 15 Hz respectively at their rated voltages. Fig. 17 shows the magnetic flux in the cross section of the machine. Centric rotor as well as different static and dynamic eccentric rotors described in section IV are studied. For each model, the space distribution of air gap flux density is extracted. Using the air gap flux density and (2) to (7), the stator back iron deflection is derived. Table III shows the cases studied using the FE modelling.

## VII. Results and Discussion

Different levels and types of rotor eccentricity are studied as described in Table III. The back iron displacement for static

TABLE III: Different designs considered in this study

| Acronym | Eccentricity | Connections PW | Connections CW | PW Short Pitch |
|---|---|---|---|---|
| C-SW-SP | Centric | Series | Series | Yes |
| C-PW-SP | Centric | Fig. 12 | Fig. 13(b) | Yes |
| SE-SW-SP | Static (Fig. 5) | Series | Series | Yes |
| SE-PW-SP | Static (Fig. 5) | Fig. 12 | Fig. 13(b) | Yes |
| SE-PW-FP | Static (Fig. 5) | Fig. 16 | Fig. 13(b) | No |
| DE-SW-SP | Dynamic (Fig. 6) | Series | Series | Yes |
| DE-PW-SP | Dynamic (Fig. 6) | Fig. 12 | Fig. 13(b) | Yes |
| DE-PW-FP | Dynamic (Fig. 6) | Fig. 16 | Fig. 13(b) | No |

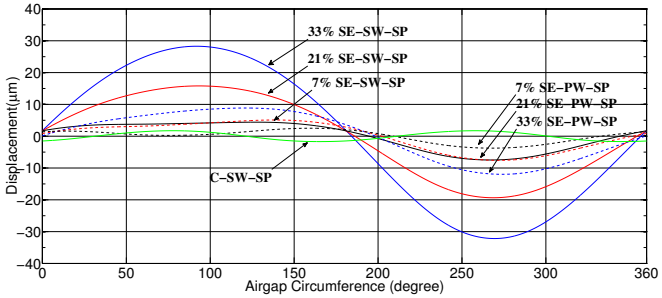


Fig. 18: Stator back iron deflection for different levels of rotor static eccentricities shown in Fig. 5

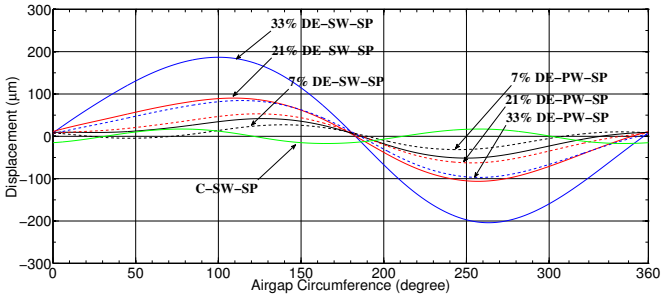


Fig. 19: Stator back iron deflection for different levels of rotor dynamic eccentricities shown in Fig. 6

(Fig. 5) and dynamic (Fig. 6) eccentricities are shown in Figs. 18 and 19, respectively, for series and parallel connected short-pitched windings. Figs. 20 and 21 compare the effect of higher number of parallel paths in reducing deflection. The *rms* value of the deflection and its reduction as the result of parallel windings for different eccentricity levels are shown in Tables IV and V for static and dynamic eccentricities, respectively.

Significant reduction can be observed in the stator back iron displacement when parallel windings are employed. As shown in Tables IV and V, a reduction of between 55% to 80% in the displacement from static eccentricity can be achieved using parallel winding designs. The level of reduction is between 40

TABLE IV: The *rms* value of deflection obtained from FE modelling for static eccentricity.

| Level of Eccentricity | Displacement($\mu m$) SE-SW-SP | SE-PW-SP | SE-PW-FP | Reduction % SW-PW-SP | SE-PW-FP |
|---|---|---|---|---|---|
| 33% | 214 | 73 | 45 | 34% | 21% |
| 21% | 125 | 43 | 28 | 35% | 23% |
| 7% | 43 | 19 | 16 | 45% | 37% |

TABLE V: The *rms* value of deflection obtained from FE modelling for dynamic eccentricity.

| Level of Eccentricity | Displacement($\mu m$) DE-SW-SP | DE-PW-SP | DE-PW-FP | Reduction % DE-PW-SP | DE-PW-FP |
|---|---|---|---|---|---|
| 33% | 137 | 62 | 26 | 45% | 19% |
| 21% | 67 | 38 | 21 | 56% | 31% |
| 7% | 29 | 17 | 14 | 58% | 49% |

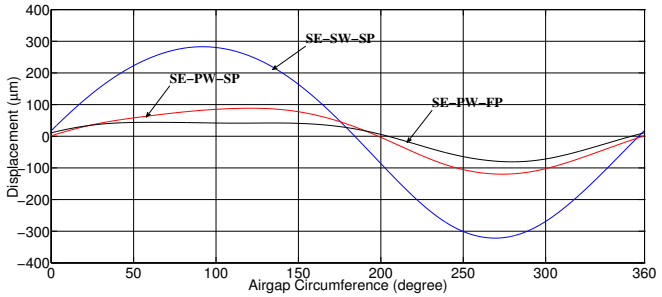


Fig. 20: Deflection in stator back iron for 33% static rotor eccentricity

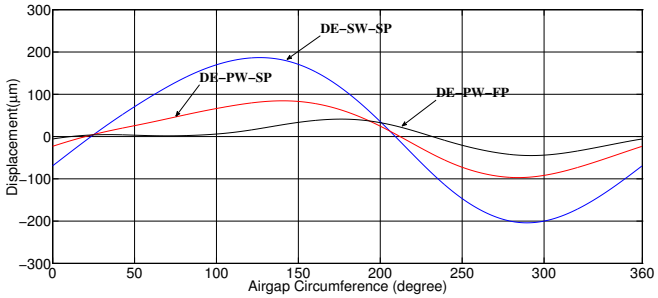


Fig. 21: Deflection in stator back iron for 33% dynamic rotor eccentricity

to 80 % for dynamic eccentricity. In addition, it can be noted from Figs. 20 and 21 that higher number of parallel paths in the PW can further suppress displacement especially when dynamic eccentricity exists.

## VIII. Conclusions

This paper has studied the practicality of parallel winding designs in the BDFM such that the direct coupling between the two stator windings and with undesirable rotor field harmonics are eliminated. This is particularly important when short pitched windings are utilized. It has been shown that with appropriate connection of coil groups in series and parallel, direct coupling of stator windings can be removed. There may be several possibilities of practical parallel winding designs, in which case the design with more parallel paths is shown to have stronger effect in suppressing the UMP.

Larger scale BDFMs are likely to be designed for slower natural speeds, hence with higher stator pole numbers. This will provide more possibilities for parallel connection of stator coils, but the practicality of such designs must be carefully assessed. The study presented in this paper, though is shown for a specific BDFM with 4 and 8 pole stator windings and a nested loop rotor, can be generalized for other BDFM designs.

## Acknowledgment

The research leading to these results has received funding from the European Union's Seventh Framework Program managed by REA Research Executive Agency (FP7/2007 2013) under Grant Agreement N.315485.

## References

[1] H. Arabian-Hoseynabadi, H. Oraee, and P. J. Tavner, "Wind turbine productivity considering electrical subassembly reliability," *Renewable Energy*, no. 35, pp. 190–197, 2010.

[2] P. C. Roberts, R. A. McMahon, P. J. Tavner, J. M. Maciejowski, and T. J. Flack, "Equivalent circuit for the brushless doubly fed machine (bdfm) including parameter estimation and experimental verification," *Electrical Power Applications, IEE Proceedings*, vol. 152, no. 4, pp. 933–942, July 2005.

[3] R. A. McMahon, X. Wang, E. Abdi-Jalebi, P. J. Tavner, P. C. Roberts, and M. Jagiela, "The bdfm as a generator in wind turbines." 12th International Power Electronics and Motion Control Conference, EPE-PEMC, September 2006.

[4] D. Dorrell, A. knight, and R. Betz, "Issues with the design of brushless dounly-fed reluctance machines: unbalanced magnetic pull, skew and iron losses." IEEE Int. Electric Machines and Drives Conf (IEMDC), 2011, pp. 663 – 668.

[5] T. Logan, R. McMahon, and K. Seffen, "Noise and vibration in brushless doubly fed machine and brushless doubly fed reluctance machine," *IET Electric Power Applications*, vol. 7, pp. 1 – 10, 2014.

[6] R. Hellmund, "Series versus parallel windings for a.c machines." Electrical World, 49:388-389, 1907.

[7] A. Burakov and A. Arkkio, "Comparison of the unbalanced magnetic pull mitigation by the parallel paths in the stator and rotor windings," *IEEE Transactions on Magnetics*, vol. 43, pp. 4083 – 4088, 2007.

[8] D. Dorrell and A. Smith, "Calculation of u.m.p in induction motors with series or parallel winding connections," *IEEE Transactions on Energy Conversion*, vol. 9, pp. 304 – 310, 1994.

[9] M. DeBortoli, S. Salon, and C. Slavik, "Effects of rotor eccentricity and parallel windings on induction machine behaviour: A study using finite element analysis," *IEEE Transactions on Magnetics*, vol. 29, pp. 1676 – 1682, 1993.

[10] D. Zarko, D. Ban, I. Vazdar, and V. Jaric, "Calculation of unbalanced magnetic pull in a salient pole synchronous generator using finite-element method and measured shaft orbit," *IEEE Transactions on Industrial Electronics*, vol. 59, pp. 2536 – 2548, 2012.

[11] J. Li, D. Choi, and Y. Cho, "Analysis of rotor eccentricity in switched reluctance motor with parallel winding using fem," *IEEE Transactions on Magnetics*, vol. 45, pp. 2851 – 2854, 2009.

[12] D. Dorrell and D. Ionel, "Radial forces and vibrations in permanent magnet and induction machines." IEEE Power and Energy Society General Meeting, 2012, pp. 1 – 6.
[13] F. Runcos, R. Carlson, N. Sadowski, P. Kuo-Peng, and H. Voltolini, "Performance and vibration analysis of a 75 kw brushless doubly-fed induction generator prototype." IEEE Industry Application Conference, 2006, pp. 2395 – 2402.
[14] A. Stavrou and J. Penman, "Modeling dynamic eccentricity in smooth air-gap induction machines." IEEE Int. Electric Machines and Drives Conf (IEMDC), 2001, pp. 864 – 871.
[15] R. Robinson, "The calculation of unbalanced magnetic pull in synchronous and induction motors," *AIEE Trans*, vol. 62, pp. 620 – 624, 1943.
[16] M. Berman, "On the reduction of magnetic pull in induction motors with off-centre rotor." IEEE Industrial Application Society Annual Meeting, 1993, pp. 343 – 350.
[17] R. Perers, U. Lundin, and M. Leijon, "Saturation effects on unbalanced magnetic pull in a hydroelectric generator with an eccentric rotor," *IEEE Transactions on Magnetics*, vol. 43, no. 10, pp. 3884 – 3890, 2007.
[18] L. Wang, R.Cheung, Z. Ma, J. Ruan, and Y. Peng, "Finite element analysis of unbalanced magnetic pull in a parge hydro generator under practical operations," *IEEE Transactions on Magnetics*, vol. 44, no. 6, pp. 1558 – 1561, 2009.
[19] R. McMahon, P. Tavner, E. Abdi, P. Malliband, and D. Barker, "Characterising brushless doubly fed machine rotors," *IET Electric Power Applications*, vol. 7, pp. 535 – 543, 2013.
[20] R. A. McMahon, E. Abdi, P. Malliband, S. Shao, M. E. Mathekga, and P. J. Tavner, "Design and testing of a 250 kw brushless dfig." Bristol, UK: 6th IET International Conference on Power Electronics, Machines and Drives (PEMD), March 2012.
[21] B. Heller and V. Hamata, *Harmonic Field Effects in Induction Machines*. Elsevier Scientific Publishing Company, 1977.
[22] P. Alger, *The Nature of Polyphase Induction Machines*. New York: John Wiley and Sons, 1951.
[23] J. Pyrhonen, T. Jokinen, and V. Hrabovcova, *Design of rotating electrical machines*. Finland: John Wiley & Sons Inc., 2007.
[24] F. Blazquez, C. Veganzones, D. Ramirez, and C. Platero, "Characterization of the rotor magnetic field in a brushless doubly-fed induction machines," *IEEE Transactions on Energy Conversion*, vol. 24, no. 3, pp. 599 – 607, 2009.
[25] E. Abdi, R. McMahon, P. Malliband, S. Shao, M. Mathekga, P. Tavner, S. Abdi, A. Oraee, T. Long, and M. Tatlow, "Performance analysis and testing of a 250 kw medium-speed brushless doubly fed induction generator," *Renewable Pawer Generation, IET*, vol. 7, no. 6, pp. 631 – 638, 2013.

**Salman Abdi** received his BSc degree from Ferdowsi University, Mashhad, Iran, in 2009 and M.S.c degree from Sharif University of Technology in 2011, both in electrical engineering. He is currently working toward the PhD degree at Cambridge University in electrical machines design and modelling. His main research interests include electrical machines and drives for renewable power generation

**Ehsan Abdi** (SM' 2012) received his BSc degree from Sharif University of Technology in 2002 and his MPhil and PhD degrees from Cambridge University in 2003 and 2006 respectively, all in Electrical Engineering. Currently, he is the Managing Director of Wind Technologies Ltd where he has been involved with commercial exploitation of the brushless doubly fed induction generator technology for wind power applications. His main research interests include electrical machines and drives, renewable power generation, and electrical measurements and instrumentation.

**Richard McMahon** received the degrees of BA (in Electrical Sciences) and PhD from Cambridge University in electrical engineering, in 1976 and 1980 respectively. Following postdoctoral work on semiconductor device processing he was appointed University Lecturer in Electrical Engineering at Cambridge University Engineering department in 1989 and became a Senior Lecturer in 2000. His research interests include electrical drives, power electronics and semiconductor materials.